A DYNAMIC CRACK GROWTH SIMULATION USING COHESIVE ELEMENTS

M. Anvari[1(*)], C. Thaulow[1] and I.Scheider[2]
[1] Department of Engineering Design and Materials, NTNU, Trondheim, Norway
[2] GKSS Research Center, Geesthacht, Germany

ABSTRACT

Rate-sensitive and triaxiality-dependent cohesive elements are used to simulate crack growth under dynamic loading conditions. To consider the effect of stress triaxiality and strain rate on the cohesive properties, a single plane strain element obeying the constitutive equations of a rate-dependent Gurson type model has been used. The single element is loaded under various stress biaxiality ratios and strain rates and the obtained stress-displacement curves are considered as traction separation law for the cohesive elements. These curves are used for analyzing a middle-cracked tension M(T) specimen made of aluminum alloy 6XXX series. The effects of constraint and strain rate on the energy absorption of the specimen and crack growth are discussed.

Introduction

Local approaches have wide application in numerical simulation of crack growth. Two local approaches, named complete Gurson model [1] and cohesive zone model [2] have been employed in the present article.

Cohesive elements used in simulating ductile fracture are supposed to represent the mechanism of nucleation, growth and coalescence of microscopic voids that initiate at the inclusions and second phase particles. The idea of the present contribution is to obtain the cohesive properties by studying the mechanical response of a single element obeying a rate-dependent Gurson type constitutive equation. This sort of mechanism-based cohesive model has also been proposed by other authors, e.g. [3,4]. It is well known that the cohesive strength increases with strain rate ([5-7]) and this implies an increase in stress triaxiality [8,9]. Using a Gurson type model provides a mean for exploring the effect of stress triaxiality on the cohesive parameters [3]. Rate sensitivity of the cohesive zone is determined by applying different values of loading speed on the rate-sensitive single element and calculating the traction separation law (TSL) parameters from the mechanical response. A similar procedure is performed by applying different stress ratios on the single element to study the effect of stress trixiality on the cohesive parameters. The shape of the TSL, cohesive strength and critical displacement are fitted to meet the results of the single element calculations for various strain rates and triaxialities. The parameters are then used for crack growth simulations of an aluminum middle-cracked tension M(T) specimen. The mechanical response of the structure is shown by the load-displacement diagrams and the results are discussed. The influence of dynamic loading on plastic energy dissipation and crack growth is illustrated, too.

To simulate the mechanical response of a structure subjected to high rate of loading, phenomena like stress waves, inertia, rate sensitivity of material and adiabatic heating need to be considered. In the presented simulations, the cohesive elements are triaxiality- and rate-dependent simultaneously. Since the values of strain rate and stress triaxiality are not available in the cohesive elements, they are calculated and transferred from the solid elements adjacent to them during transient dynamic analyses. While rate dependency and constraint are considered for the cohesive elements, the influence of inertia and elastic waves on bulk material is inherent in the transient dynamic analyses. The influence of adiabatic heating has not been considered in the analyses.

The analyses are performed in ABAQUS/Standard nonlinear finite element code [10]. The rate-dependent complete Gurson model developed and implemented into ABAQUS as a user defined material (UMAT) subroutine [11] is used for the single element calculations. The cohesive element calculations are performed by a user defined element (UEL) subroutine developed by Scheider [12] and expanded by the present authors for rate and triaxiality-dependent cohesive elements to be used in transient dynamic analysis.

* Present address: Det Norske Veritas, Performance Assurance & System Integrity, P.O. Box 7400, Bergen, Norway

Calculations

The following equation [13] was employed to calculate rate dependency of the bulk material:

$$\overline{\sigma} = \sigma_0 \left(1 + \frac{\overline{\varepsilon}}{\varepsilon_0}\right)^N \left(\frac{\dot{\overline{\varepsilon}}}{\dot{\varepsilon}_0}\right)^m \tag{1}$$

where $\overline{\sigma}$, $\overline{\varepsilon}$, σ_0 and ε_0 stand for true stress, true plastic strain, yield stress, and a reference strain respectively. $\dot{\overline{\varepsilon}}$ and $\dot{\varepsilon}_0$ are the strain rate and a reference strain rate, respectively. N is known as strain hardening and m as strain rate hardening exponent. In this formulation, the strength of the material increases with the increase of strain rate. The constitutive behavior is based on von Mises plasticity with pure isotropic hardening. Viscous, i.e. time dependent effects are not considered. The values considered for aluminum 6XXX series are: σ_0 =217 MPa, ε_0 =0.002, $\dot{\varepsilon}_0$ =150 1/s, N =0.0526, m =0.05. Mass density of aluminum, ρ =2700 Kg/m^3 has been considered in all of the calculations.

The unit cell considered in the present study is a four node plane strain element obeying rate-dependent complete Gurson model as the constitutive equation. Rate sensitive bulk material is described by Equation (1). Details on formulation and implementation of rate-dependent Gurson type models are found elsewhere [14,15]. The initial void volume fraction of f_0 = 0.002 is considered in the calculations as suggested in [16], since no experimental data on micromechanical information is available for this parameter. The analyses are performed for an element with the initial size of *DxD*=1 mm^2, for different stress biaxialities β, as shown in Figure 1:

$$\beta = \frac{\sigma_{11}}{\sigma_{22}} \tag{2}$$

where σ_{11} and σ_{22} are the stresses in x and y directions, respectively. If the material is incompressible, the stress triaxiality which is the ratio between mean normal stress and von-Mises equivalent stress is given by [3]:

$$H \approx \frac{1+\beta}{\sqrt{3}(1-\beta)} \tag{3}$$

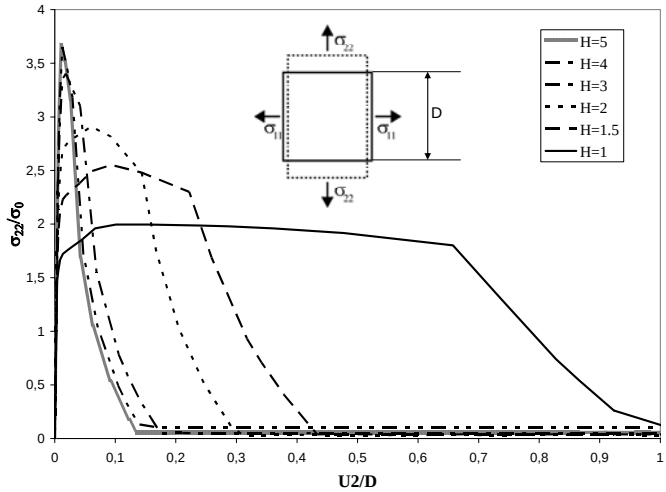

Figure 1. The effect of stress triaxiality on the traction separation behavior of a unit cell

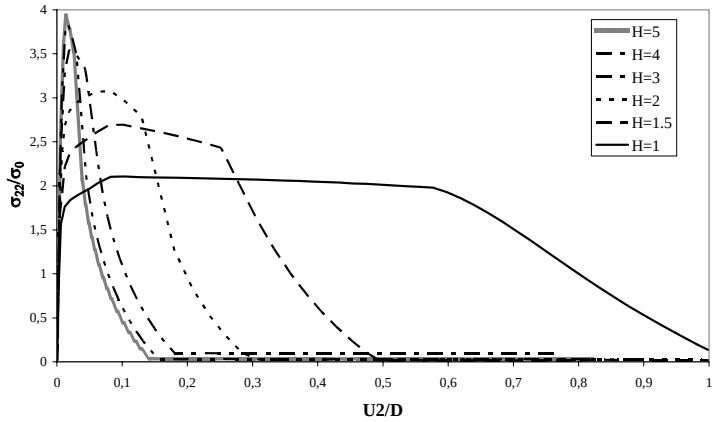

Figure 2. The effect of stress triaxiality on the traction separation behavior of a rate dependent unit cell subjected to strain rate of 500 1/s

In order to investigate the effect of strain rate on stress-elongation behavior, quasi-static analyses were performed with a rate-dependent model and high speed loading. Figure 2 shows the normalized traction separation behavior for different triaxialities for a loading rate of 500 mm/s or in other words, an initial strain rate of 500 1/s for an element of initial length *D*=1 mm. To check the effect of strain rate while triaxiality does not change, various loading speeds were applied for the same triaxiality of 1.5 (β =0.44). Figure 3 shows that the curves are almost parallel and only the value of strength changes for the same maximum displacement. Figure 4 shows the curves fitted to the calculated values of strength and energy for the rate-dependent case at constant loading rate (V=500 mm/s) and different triaxiality values. Figure 5 shows how the values of cohesive strength and cohesive energy change with loading rate for a constant triaxiality of 1.5. As it is shown, the value of the maximum traction changes as a function of the rate independent case for the same triaxiality multiplied by the relative strain rate to the power of *m* (strain rate hardening exponent).

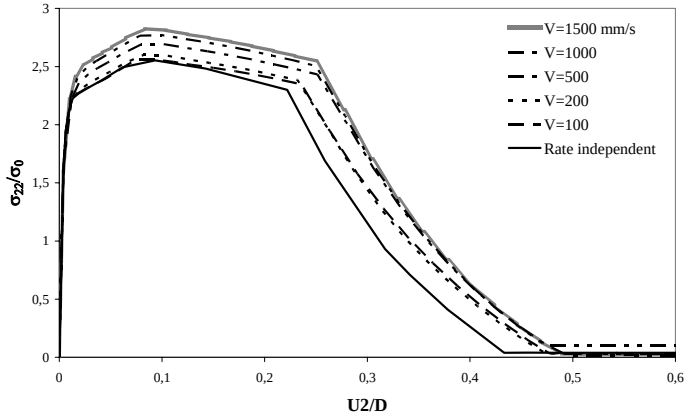

Figure 3. Traction separation behavior st different load speeds (strain rates) and constant stress triaxiality (H=1.5)

The traction separation law introduced by Scheider and Brocks [17] has been used to reproduce the calculated damage and failure of the unit cell by a cohesive element. This TSL has the following form:

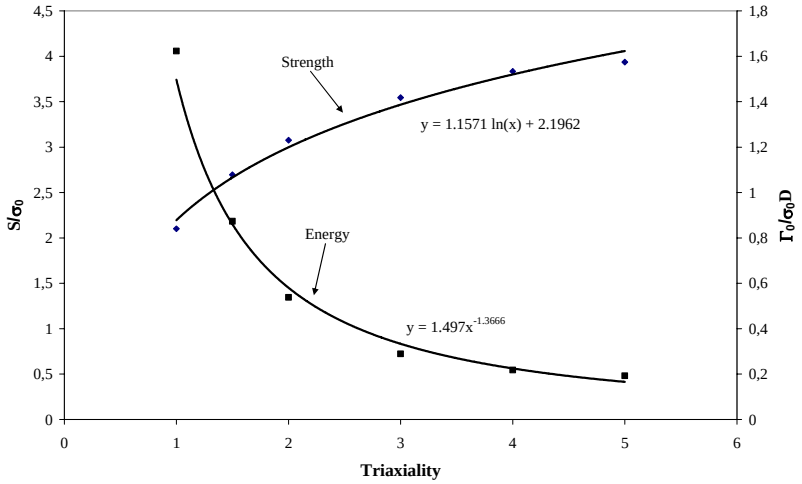

Figure 4. Variation of normalized cohesive strength and energy vs. stress triaxiality in constant load speed of 500 mm/s

$$T = S\begin{cases} 2\left(\dfrac{\delta}{\delta_1}\right)-\left(\dfrac{\delta}{\delta_1}\right)^2 & ,0<\delta<\delta_1 \\ 1 & ,\delta_1<\delta<\delta_2 \\ 2\left(\dfrac{\delta-\delta_2}{\delta_0-\delta_2}\right)^3-3\left(\dfrac{\delta-\delta_2}{\delta_0-\delta_2}\right)^2+1 & ,\delta_2<\delta<\delta_0 \end{cases} \tag{4}$$

where T and δ are the traction and opening of the cohesive element, respectively. S is the maximum traction (cohesive strength) and δ_0 is the maximum opening (critical separation). δ_1 and δ_2 are shape parameters. In this formulation, critical opening is:

$$\delta_0 = \frac{2\Gamma_0}{S}\frac{1}{1-\frac{2}{3}\frac{\delta_1}{\delta_0}+\frac{\delta_2}{\delta_0}} \tag{5}$$

where Γ_0 is the energy absorbed by cohesive elements, known as cohesive energy.

Using the mathematical expressions shown in Figures 7 and 8, the following approximations are obtained for the cohesive strength and energy:

$$\frac{\Gamma_0}{D} \approx 1.43H^{-1.36}\,\sigma_0\left(\frac{\dot{\bar{\varepsilon}}}{\dot{\varepsilon}_0}\right)^m \tag{6}$$

$$S \approx \left(1.1\ln(H)+2.1\right)\sigma_0\left(\frac{\dot{\bar{\varepsilon}}}{\dot{\varepsilon}_0}\right)^m \tag{7}$$

where H is the stress triaxiality and D is the characteristic length scale of the Gurson model, which is usually based on the micromechanical structure of the material. A value of D=0.1 mm is chosen in accordance to [18] who also investigated an aluminum alloy of 6XXX series. Considering e.g. Figure 2, it is recognized that the piecewise TSL defined by Equation (4) fits properly to the curves if the shape parameters δ_1 and δ_2 are adjusted accordingly. Combining Equations (5), (6) and (7), the critical separation reads:

$$\frac{\delta_0}{D} \approx \frac{2.8H^{-1.36}}{1.1\ln(H)+2.1}\frac{1}{1-\frac{2}{3}\frac{\delta_1}{\delta_0}+\frac{\delta_2}{\delta_0}} \tag{8}$$

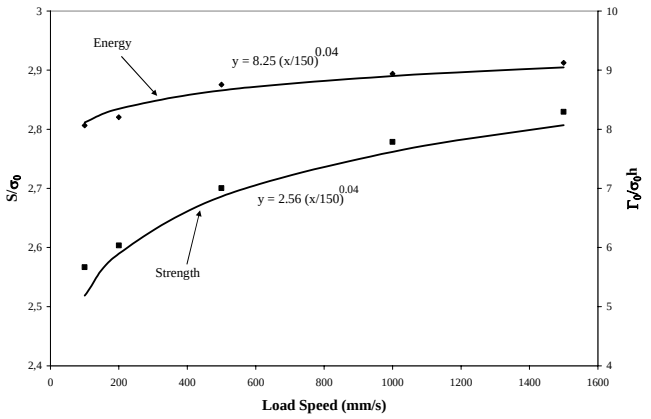

Figure 5. Variation of normalized cohesive strength and energy vs. load speed for constant triaxiality of 1.5

The comparison between the stress elongation behavior obtained from rate-dependent Gurson model calculations and the TSL approximation of Equation (4) with the cohesive parameters $\frac{\delta_1}{\delta_0}$=0.07 and $\frac{\delta_2}{\delta_0}$=0.35 are shown in Figure 6 for two different triaxiality values. Since the curves obtained from the single element calculations and those based on Equation (4) are not exactly the same, the critical displacements are a slightly different for the same cohesive strength and energy, but the differences are reasonable.

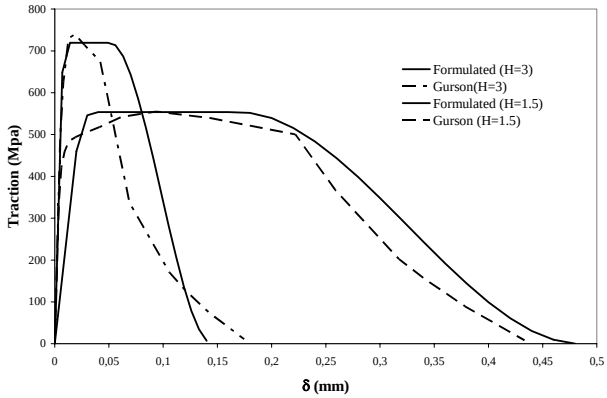

Figure 6. Comparison between traction separation behavior obtained from Gurson type model and the TSL proposed in Equation (4)

Crack growth simulations and results

An M(T) specimen of unit thickness and dimensions of 100×100 mm^2 has been modeled using four node plane strain elements. The ratio of the initial crack length to the specimen's width is a/W = 0.5. One row of cohesive elements with initial zero height has been used at the ligament. Because of symmetry, one fourth of the specimen has been modeled. Figure 7 shows the specimen and the detailed mesh at the crack tip and a part of the ligament. The smallest continuum element size belongs to the elements adjacent to the ligament and it is 0.1×0.1 mm^2. The surrounding continuum elements behave according to Equation (1) and the cohesive elements based on Equations (4), (6), (7) and (8). Each cohesive element possesses four nodes and two integration points. For each cohesive element, the actual values of nodal displacement, triaxiality and strain rate are used to compute the current value of traction and element stiffness. The values of triaxiality and strain rate are calculated in the continuum elements along the ligament at all of the integration points using UVARM subroutine in ABAQUS. The averages of these values are then calculated after the load increment and provided to the respective

adjacent cohesive elements in the next increment as shown in Figure 8. The error of this kind of explicit scheme is accepted since the time increments are always chosen to be small enough.

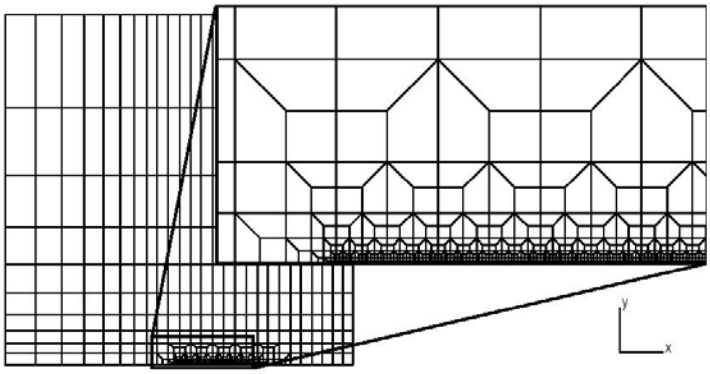

Figure 7. M(T) specimen and the detailed finite element model of the crack tip area

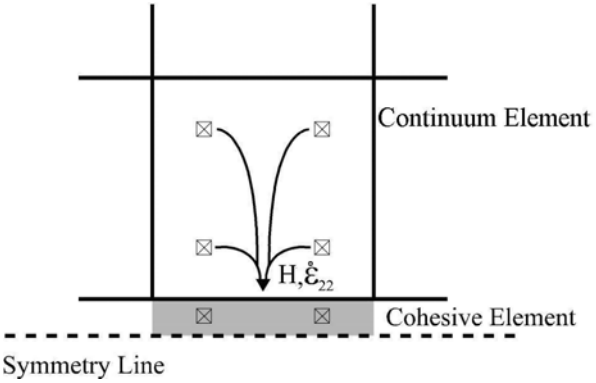

Figure 8. Triaxiality and strain rate values are transferred to the cohesive elements from the adjacent continuum elements

Material separation process involving void growth and plastic deformation at microlevel are irreversible by nature. This property has been implemented in the cohesive element formulation so that a separation already happened to an element remains after local unloading and relaxing the stress [12].

The analyses are aimed to evaluate the influence of constraint, rate sensitivity, inertia and elastic waves on the energy absorbed by the specimen. In the analyses, the effects of inertia and elastic waves are investigated as well as the influence of stress triaxiality and rate sensitivity. It should be reminded that in the calculation of the energy of separation, only the effect of sensitivity and constraint have been considered. The load is applied as a prescribed displacement at the upper edge of the specimen with the speed of 3.3 m/s. The load and displacements presented in the following diagrams are the values calculated on the boundary of the model. Figure 9 shows the load-displacement curves obtained from the analyses. The existence of the oscillations is inevitable due to the existence of elastic waves. The time that elastic waves travel the length of the specimen is around 20 μs; that is much shorter than the total time of fracture (the shortest time of fracture is 131.8 μs, which is for the case of rate dependent bulk material). The elastic waves can have two sources, one is the dynamically applied load and the other is the wave induced by broken cohesive elements or, in other words, the waves induced because of the relatively high speed of the crack growth. Because of the implicit integration used in the dynamic analyses, there is no severe limitation on the time increment chosen.

Dynamic simulation considering the rate dependency only for bulk material leads to the most conservative assumption. Ignoring the effect of strain rate and triaxiality on the behavior of interface elements makes the results unrealistic. Using rate- and triaxiality-dependent cohesive elements results in more energy absorption, although it is less than the simulation which ignores all of these influences. Figure 10 shows the crack growth vs. time for dynamic simulations. In all of the cases, the crack speed is low in the beginning and then it increases to a somewhat steady state speed. The case with no rate dependency is an exception in which it seems that the crack speed is changing during the growth. The figure shows clearly that the steady state speed of the crack growth is highest, about 1430 m/s, for the case in which only bulk material is rate

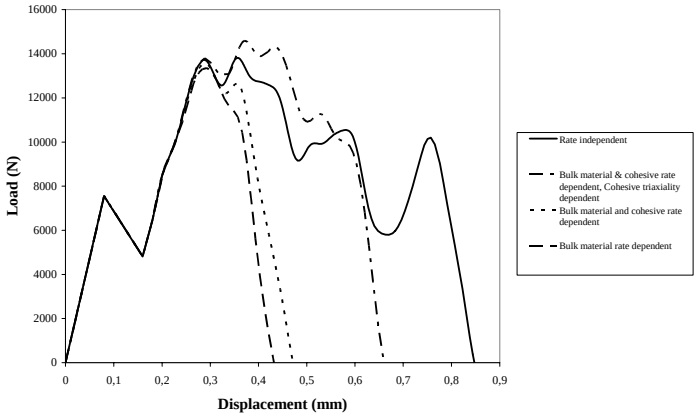

Figure 9. The effect of strain rate and constraint on the load-displacement behavior

dependent, the crack growth initiation happens almost at the same time as for the case with no rate dependency. This is in contrast to the investigations of Basu [19] who numerically showed that strain rate sensitivity plays a beneficial role on dynamic ductile fracture initiation. This contradiction is related to ignoring triaxiality change even at the first stages of deformation. It is observed in Figure 10 that when triaxiality dependency is considered, crack growth initiation happens at 69 μs which is higher than the rate-insensitive case. To check if this effect is due to the rate sensitivity of the material, a dynamic case was simulated with triaxiality dependent cohesive elements while no rate sensitivity was considered. The analysis showed that the crack growth initiation happened at 61.8 μs. This proves that rate sensitivity has postponed crack growth initiation, although after a short time, crack growth speed is higher than the rate-insensitive case. It should also be noted that in the case where stress triaxiality change has been ignored, the crack growth velocity becomes so high that the assumption of ductile mechanism of crack growth might be inaccurate. It is worth noting that for the case in which only rate dependency of bulk material has been considered, the crack speed is around 1400 m/s. In this case, the inertia effect on fracture energy is important, but it has been ignored in the calculation. Regarding these discussions and back to Figure 9, it is well understood why the load in the triaxiality and rate dependent case is higher in the beginning and drops very fast after some time. The reason why crack speed is much higher in the case of rate-dependent plasticity is that the material hardens due to high loading rate and opens the crack (cohesive elements) more easily.

When the cohesive zone is rate dependent, the cohesive strength is increased at high loading rates and this causes more energy dissipated by plasticity in the surrounding material. Although the stresses needed for crack propagation are higher compared to the case with rate independent cohesive parameters, the cohesive strength, S, is not high enough to decrease the crack growth rate as much as for the rate insensitive case. The reason is that with increasing plasticity, the crack opening speed decreases, so the local strain rate and consequently the cohesive strength decrease again. Besides, stress triaxiality

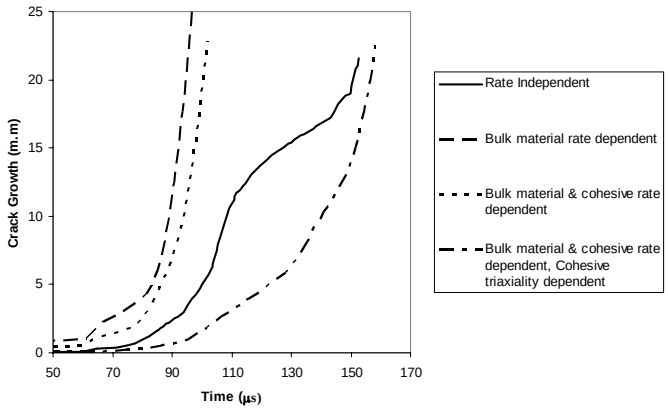

Figure 10. The effect of strain rate and constraint on the load-displacement behavior

increases initially, but because of inertia it decreases while the crack is growing [20]. This means that the decrease of the cohesive strength is related to the inertia. Figure 11 shows the change of triaxiality value during crack growth for the case in which rate dependency and triaxiality have been considered for the cohesive elements.

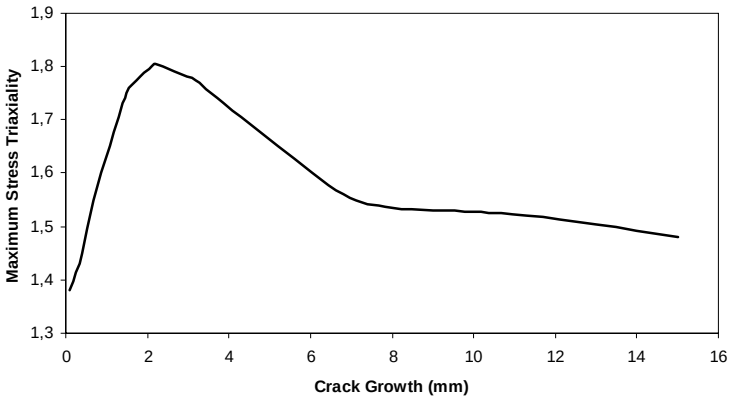

Figure 11. The change of stress triaxiality during crack growth under dynamic loading conditions

Conclusions

The effects of triaxiality and strain rate on cohesive properties have been considered simultaneously in a finite element dynamic crack growth simulation. The results show that in dynamic conditions, the value of stress triaxiality increases initially whereas inertia leads to its decrease during the crack growth. It is shown that considering strain rate in the dynamic simulations while ignoring the stress triaxiality leads to a high underestimation of the toughness. The analyses also show that although strain rate sensitivity makes a ductile crack initiation to be postponed, it leads to a faster crack growth due to a decrease in the amount of plasticity at the crack tip area. In other words, although the energy absorption increases initially, it drops very fast after a short crack growth. This is in contrast with a dynamically loaded uncracked specimen, where positive strain rate sensitivity always makes the specimen absorb more energy.

Acknowledgments

The authors from NTNU would like to acknowledge Hydro Aluminium and the Research Council of Norway for their support through the NorLight project.

References

1. Z.L. Zhang, C. Thaulow, and J. Ødegård. A complete Gurson model approach for ductile fracture. Engineering Fracture Mechanics, **67**:155–168, 2000.
2. A. Needleman. A continuum model for void nucleation by inclusion debonding. Journal of Applied Mechanics, **54**:525–531, 1987.
3. T. Siegmund and W. Brocks. Predictions of the work of separation and implications to modeling. International Journal of Fracture, **99**:97–116, 1999.
4. V. Tvergaard. Crack growth predictions by cohesive zone model for ductile fracture.Journal of the Mechanics and Physics of Solids, **49**:2191–2207, 2001.
5. F. Costanzo and J.R. Walton. Numerical simulations of a dynamically propagating crack with a nonlinear cohesive zone. International Journal of Fracture, **91**:373–389, 1998.
6. A. Corigliano and M. Ricci. Rate-dependent interface models: formulation and numerical applications. International Journal of Solids and Structures, **38**:547–576, 2001.
7. X. Zhang, Y.W. Mai, and R.G. Jeffrey. A cohesive plastic and damage zone model for dynamic crack growth in rate-dependent materials. International Journal of Solids and Structures, **40**:5819–5837, 2003.
8. K.B. Broberg. Influence of T-stress, cohesive strength and yield strength on the competition between decohesion and plastic flow in a crack edge vicinity. International Journal of Fracture, **100**:133–142, 1999.
9. M.P. Wnuk and J. Legat. Work of fracture and cohesive stress distribution resulting from triaxiality dependent cohesive zone model. International Journal of Fracture, **114**:29–46, 2002.
10. ABAQUS. ABAQUS Version 6.4. H.K.S. Inc. Pawtucket, U.S.A., 2003.

11. Z.L. Zhang. A practical micro-mechanical model-based local approach methodology for the analysis of ductile fracture of welded T-joints. Lappeenranta University of Technology, Finland, Ph.D. Thesis, 1994.
12. I. Scheider. Cohesive model for crack propagation analyses of structures with elastic plastic material behavior. Foundations and implementation. Technical report, GKSS internal report no. WMS/2000/19, 2000.
13. J. Pan, M. Saje, and A. Needleman. Localization of deformation in rate sensitive porous plastic solids. International Journal of Fracture, **21**:261–278, 1983.
14. A. Needleman and V. Tvergaard. An analysis of dynamic, ductile crack growth in a double edge cracked specimen. International Journal of Fracture, **49**:41–67, 1991.
15. D. Z Sun, A. H¨onig, W. B¨ohme, and W. Schmitt. Application of micromechanical models to the analysis of ductile fracture under dynamic loading. In F. Erdogan and R.J. Hartranft, editors, Fracture Mechanics: 25th Syp., ASTM STP 1220, pages 343–357, American Society for Testing and Materials, Philadelphia, 1994.
16. G. Bernauer and W. Brocks. Micro-mechanical modelling of ductile damage and tearing- results of a European numerical round robin.. Fatigue and Fracture of Engineering Materials and Structures, **25**:363-384, 2002.
17. I. Scheider and W. Brocks. Simulation of cup-cone fracture using the cohesive model. Engineering Fracture Mechanics, **70**:1943–1961, 2003.
18. P. Negre, D. Steglich, and W. Brocks. Crack extension in aluminium welds: a numerical approach using the gurson-tvergaard-needleman model. Engineering Fracture Mechanics, **71**:2365–2383, 2004.
19. S. Basu and R. Narashimhan. Finite element simulation of mode I dynamic, ductile fracture initiation. International Journal of Solids and Structures, **33(8)**:1191–1207, 1996.
20. S. Basu and R. Narashimhan. A numerical investigation of loss of crack tip constraint in a dynamically loaded ductile specimen. Journal of the Mechanics and Physics of Solids, **48**:1967–1985, 2000.